Reactions of Metastable Argon Atoms with Molecular Hydrogen at 300 and 80 K: Origin of the Ultraviolet Chemiluminescence

N. Sadeghi,* D. W. Setser, and M. Touzeau†

Laboratoire de Spectrométrie Physique (UMR CNRS 5588), Université Joseph Fourier-Grenoble I. BP 87, 38402 St. Martin d'Héres Cedex, France

Received: January 9, 2002; In Final Form: April 18, 2002

The reactions of $Ar(4s^3P_2)$ and $Ar(4s'^3P_0)$ metastable atoms with H_2 and D_2 have been studied at 300 and 80 K by the stationary and flowing-afterglow techniques. Total quenching constants were measured for both metastable atoms for H_2 and D_2 at 300 K and for H_2 at 80 K. Optical pumping in the stationary-afterglow experiment was used to select one or the other metastable atoms, and chemiluminescence spectra were obtained for state-selected metastable atoms reacting with H_2 and D_2. The branching fractions for chemiluminescence, which range from 0.07 to 0.30, are higher for D_2 than H_2 and higher for $Ar(4s'^3P_0)$ atoms than for $Ar(4s^3P_2)$ atoms. The chemiluminescence is assigned to the $ArH(B^2\Pi-X^2\Sigma^+)$ and $ArD(B^2\Pi-X^2\Sigma^+)$ transitions. The total quenching rate constants for H_2 decline by factors of 80 and 30 at 80 K, relative to the room-temperature values, for the reactions of $Ar(4s^3P_2)$ and $Ar(4s'^3P_0)$ atoms, respectively. Both the chemiluminescence and dark product channels of these reactions probably proceed by chemical reaction rather than by electronic energy transfer.

I. Introduction

The reactions of $Ar(4s^3P_2)$, 11.55 eV, and $Ar(4s'^3P_0)$, 11.72 eV, metastable atoms with H_2 and D_2 were investigated 20 years ago[1−4] as part of a general effort to measure rate constants and product distributions from reactions of electronically excited metastable rare gas atoms.[1−10] The rate constants for these reactions

$$Ar(4s^3P_2 \text{ or } 4s[3/2]_2) + H_2 \rightarrow 2H + Ar \qquad (1)$$

$$Ar(4s'^3P_0 \text{ or } 4s'[1/2]_0) + H_2 \rightarrow 2H + Ar \qquad (2)$$

were established to be $(6-8) \times 10^{-11}$ cm^3 molecule^{-1} s^{-1} at room temperature.[1,9,10] However, the mechanism by which the H atoms are formed has not been formulated at the molecular level. In particular, the broad ultraviolet continuum chemiluminescence, which has a branching fraction of 0.05− 0.10 for reaction 1,[3−5] has been the source of speculation. The first suggestion for the chemiluminescence was the H_2 ($a^3\Sigma^+_g-b^3\Sigma^+_u$) continuum emission, which is commonly observed from hydrogen discharge lamps, even though the H_2 ($a^3\Sigma^+_g$; $v=0$) state is 0.27 eV above the energy of the $Ar(4s^3P_2)$ atoms. The alternative suggestion was that the chemiluminescence originated from the bound-free emission of ArH* molecules that were formed by reactive quenching.[5] The latter idea subsequently received support from observation of the same emission spectrum from the $H_2(B^1\Sigma^+_u,\ v' \geq 3)$ + Ar reaction.[11] In the present work, we will report a detailed study of reactions 1 and 2 for both H_2 and D_2 at 300 K using the stationary-afterglow technique with optical pumping to separate the $Ar(4s^3P_2)$ and $Ar(4s'^3P_0)$ concentrations to obtain the chemiluminescence spectrum from the reaction of metastable atoms in each state. These data are complemented by experiments in flow reactors to measure the total quenching constants at 300 and at 80 K. By combining all the results, rate constants and branching fractions for the chemiluminescence are reported for reactions 1 and 2 at 80 and 300 K for H_2 and D_2. The recent theoretical,[12−15] and experimental,[16−19] characterization of the states of ArH* and ArD* permits a firm conclusion to be reached in favor of a reactive quenching mechanism for reactions 1 and 2 for both the chemiluminescence and the dark, H-forming channels. The state- resolved rate constants for the two metastable atoms and for H_2 and D_2 show that the quenching mechanism is sensitive to the quantum states in the entrance channel and that these factors must be incorporated into any attempt to model the reactions.

In addition to the reactions of the metastable Ar atoms with H_2, the reactions of the resonance state atoms, $4s^3P_1$ and $4s'^1P_1$, also have been analyzed. A significant fraction of the quenching proceeds with formation of the bound $H_2(B^1\Sigma^+_u,\ v'=3,4)$ molecules.[20] However, the large rate constants[21] ($20-30 \times 10^{-11}$ cm^3 molecule^{-1} s^{-1}) require additional dark product channels, and H atoms probably are formed either directly or indirectly. The metastable and resonance states of Kr and Xe also have large rate constants for quenching by H_2,[1,22] where the only pathways are excitation transfer to the dissociative $H_2(b^3\Sigma^+_u)$ state or reactive quenching. These excited-state rare gas atom reactions have aspects in common with reactions of excited alkali metal atoms with H_2, which proceed by chemical reaction and by intra-or intermultiplet relaxation.[23,24] In addition to their fundamental importance as prototype systems for quenching of electronically excited rare gas atom by hydrogen containing molecules, reactions 1 and 2 are of practical importance in discharge systems involving H_2 and Ar.[25]

Before presenting the experimental results, we will summarize the thermochemistry for reactions 1 and 2 and the spectroscopy of the ArH* and ArD* systems. Many Rydberg states of the ArH* and ArD* molecule have been spectroscopically charac-

* Corresponding author. E-mail: nader.sadeghi@ujf-grenoble.fr.
† LPGP (UMR CNRS 8578) Université Paris-Sud-Orsay, 91405 Orsay Cedex, France.

10.1021/jp020014m CCC: $22.00
Published on Web 06/01/2002

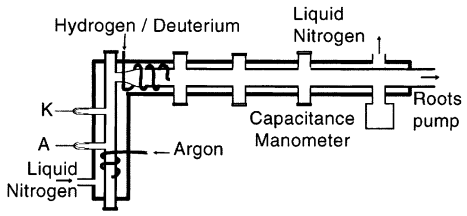

Figure 1. Schematic diagram of the low-temperature flow reactor in Orsay.

terized, and their convergence limits to ArH^+ and ArD^+ have been assigned.[16] Thus, one can use the $D^o_0(ArH^+)$ and $D^o_0(ArD^+)$ values to obtain the absolute energies of the ArH* and ArD* states relative to Ar + H(D). We used[26] $D^o_0(ArH^+) = 3.86 \pm 0.03$ and $D^o_0(ArD^+) = 3.90 \pm 0.03$ eV with the energies cited[16] for $ArH(B^2\Pi)$ and $ArD(B^2\Pi)$ to obtain excitation energies of 7.09 and 7.04 eV for $ArH(B^2\Pi)$ and $ArD(B^2\Pi)$, respectively. With the $D^o_0(H_2) = 4.478$ and $D^o_0(D_2) = 4.456$ eV values added, the threshold energies for the formation of ArH(B) and ArD(B) from Ar + H_2 (D_2) become 11.57 ± 0.03 and 11.60 ± 0.03 eV, respectively. Thus, reaction 1 would be essentially thermoneutral and reaction 2 substantially exoergic for ArH(B) or ArD(B) formation. The threshold energies for formation of the predissociated $ArH(A^2\Sigma^+)$ and $ArD(A^2\Sigma^+)$ states are much lower, 10.81 and 10.84 eV, respectively. The $C^2\Sigma^+$ states of ArH^+ and ArD^+ are within 0.003 eV of the $B^2\Pi$ states, but the C states mainly predissociate rather than fluorescence. The experimental measurements[16−18] and the theoretical calculations[14,15] of the radiative and predissociative lifetimes of the A, B, and C states of ArH* and ArD* are in accord, and we can accept that the $B^2\Pi$ states are mainly responsible for the ArH* and ArD* emission from reactions 1 and 2. The radiative lifetime of the $B^2\Pi$ state is 16.6 ± 1.2 ns, and its collisional quenching should not occur at the pressures of our experiments. Charge-exchange experiments between ArH^+ and Cs provide good ArH(B−X) emission spectra,[18] which match the calculated spectra after a slight adjustment of the theoretical ground-state potential.[13,14] Reaction channels that yield the $A^2\Sigma^+$ state would be observable only as H atom formation; the predissociation rate does decrease for ArD* molecules, and $ArD(C^2\Sigma^+)$ may contribute to the observed chemiluminescence. The most commonly observed ArH* band at 768 nm now is known to belong to the $E^2\Pi \rightarrow A^2\Sigma^+$ transition. A more complete comparison between the chemiluminescence spectra of reactions 1 and 2 and the $B^2\Pi - X^2\Sigma^+$ spectra from the charge-exchange reactions[16−18] will be presented in the Discussion.

II. Experimental Methods

The low temperature experiments were done in a flow reactor at the Orsay laboratory, which has been described previously[27] and is shown in the schematic diagram in Figure 1. The Pyrex flow tube was located inside a cooling jacket, made also of Pyrex, filled with liquid nitrogen. The flow reactor walls were maintained at about 80 K. Before entering the flow tube, both argon and hydrogen were also cooled to 80 K by passing through 6 mm diameter coiled tubes located inside the cooling jacket. The Ar($4s^3P_2$ and $4s'^3P_0$) atoms were produced by a 1 mA-dc discharge inside a 20 mm inner diameter, 40 cm long discharge tube. The reaction flow tube, 50 mm inner diameter and 65 cm long, was equipped with three pairs of quartz windows, separated about 20 cm from each others. The first pair was located immediately downstream of the H_2 injection point. The gas pressure, between 0.3 and 1 Torr, for flow rates ranging between 0.6 and 5 slm (standard liter per minute) of argon, was measured with a capacitance manometer. The hydrogen flow rate was 3 orders of magnitude smaller. Pumping with a roots blower backed by a mechanical pump, provided a linear flow velocity of about 10 m/s in the reaction flow tube at 80 K. No attempt was made to separate the two metastable concentrations in this Orsay reactor.

A 45 mm inner diameter, room-temperature flow reactor was used in the Grenoble laboratory. The design of this flow reactor and working parameters were described in earlier work.[28]

In both reactors, the concentrations of the metastable atoms was monitored by atomic absorption spectroscopy. A homemade radio frequency powered Ar lamp served as a source for the 763.5 nm ($4p[3/2]_2 \leftarrow 4s^3P_2$) and 794.8 nm ($4p'[3/2]_1 \leftarrow 4s'^3P_0$) lines used for the absorption measurements. The emission line width from this Ar lamp have been deduced from the non linearity, versus the absorbing atom density, of the absorption rate $\mathcal{A} = (I_0 - I)/I_0$ of the 763.5 nm line, where I_0 (I) refers to the intensity received by the detector in the absence (presence) of absorbing atoms.[29] When the Ar($4s^3P_2$) density is high enough, the double-path absorption rate $\mathcal{A}_{2l}$ is smaller than 2 times the single-path absorption rate $\mathcal{A}_l$. The variation of $\mathcal{A}_{2l}/\mathcal{A}_l$ versus $\mathcal{A}_l$ permits a determination of the ratio between emission and absorption line widths,[29] which allows the absorption rate to be related to the absolute atomic concentrations of $4s^3P_2$ and $4s'^3P_0$. In both flow reactors, at room temperature and in the absence of added reagent, the typical Ar($4s^3P_2$) and Ar($4s'^3P_0$) concentrations were about 1×10^{10} and 0.15×10^{10} atoms cm^{-3}, respectively. At 300 K, the bulk flow speeds in the flow reactors were in the range of 30−50 ms^{-1}. For our pressure range and in the absence of reagent, the decay of the metastable atoms densities by diffusion to and quenching at the walls and by two- and three-body collisions with argon atoms was slow enough[30] (the total loss frequency was less than 100 s^{-1}) that the loss of metastable densities between the first and the second observation windows was insignificant. The metastable atom concentrations and decay process at 80 K will be described when the quenching data are presented.

Experiments at 300 K using the stationary-afterglow method with optical pumping to isolate the $4s^3P_2$ and $4s'^3P_0$ atoms were done in the Grenoble laboratory. The experimental setup for the experiments with H_2 and D_2 differs only slightly from that used previously[31] to study the reactions of the metastable atoms with N_2. A rf pulsed electrodeless discharge (~100 μs duration, 200 pulses/s) was applied to an Ar:H_2 (D_2) = 1000:1 gas mixture for total pressures of 0.05−0.5 Torr to generate the $4s^3P_2$ and $4s'^3P_0$ atoms. The gases were contained in a cylindrical quartz cell (ϕ_i=7 cm, L=30 cm). The rf power used for the discharge was maintained at a low level, near the discharge cutoff, and the production of vibrationally excited H_2 (D_2) molecules in the ground electronic state is minimized. The electron density was also minimized so that the production in the afterglow of the resonance state Ar($4s^3P_1$) and Ar($4s'^1P_1$) atoms was negligible. The ArH*, ArD*, and $N_2(C^3\Pi_u - B^3\Pi_g)$ spectra were observed in the afterglow by a 0.6 m scanning Jobin-Yvon monochromator with a R928 (Hamamatsu) photomultiplier tube. The spectral response of the optical detection system has been calibrated using a deuterium lamp. The emission intensity signal was sent directly onto a chart recorder or stored on a multichannel analyzer and passed to a computer for analysis. Both emission and absorption measurements were made only during a 1−2 ms detection gate positioned ~1 ms after the cessation of the discharge.

One of the Ar metastable atoms ($4s^3P_2$ or $4s'^3P_0$) was selected by depopulating the other one by optical pumping, using a tunable cw dye laser pumped by a Kr^+ laser and operating with oxazine dye in multimode with a spectral bandwidth of about 0.03 Å and a power output of up to 300 mW. The laser beam was expanded before passing through the discharge cell following its axis. Using the optical absorption technique, we measured, within the detection gate, changes in $4s^3P_2$ and $4s'^3P_0$ concentrations due to the laser beam. The $4s^3P_2$ atoms were removed by laser pumping at 696.5 nm to the $Ar(4p'[1/2]_1$ or $2p_2$) level which subsequently cascades to the Ar($4s'$) levels. So that ~40% of the $4s^3P_2$ concentration can be converted to the $4s'^3P_0$ concentration, which enhances the latter by a factor 3−5. The $Ar(^3P_0)$ atoms were removed by pumping at 772.4 nm to the same $Ar(2p_2)$ state. Since the initial density of $4s'^3P_0$ atoms was less than 10% of the $4s^3P_2$ atom density, it was relatively easy to remove all of the $4s'^3P_0$ atoms. However, even the $4s^3P_2$ concentration could be reduced to 1−2% of its original value, and nearly pure $4s'^3P_0$ atoms could be obtained. The small contribution to the spectra from the remaining $4s^3P_2$ concentration could be subtracted and pure spectra from $4s'^3P_0$ are reported. Additional information about the optical pumping technique is given in refs 8, 28, and 29.

III. Experimental Results

A. Flow Reactor Measurements: Room-Temperature Quenching Rate Constants. The total quenching rate constants at 300 K for reactions 1 and 2 were measured for H_2 and D_2 in the Grenoble flow reactor. In each case the $4s^3P_2$ and $4s'^3P_0$ atom concentrations were determined by atomic absorption spectroscopy at a fixed point, 44 cm downstream from the reagent (N_2, H_2, and D_2) inlet. Since the reagent concentration greatly exceeds the metastable atom concentrations, the integrated rate law has the form given in eq3,

$$\mathrm{Ln}[\mathrm{Ar}\,(4s^3P_J)]\alpha\,(k_{\mathrm{Ar}} + k_Q[Q])\,t \qquad (3)$$

where k_{Ar} is the total first-order decay constant in the absence of added reagent, Q, and k_Q is the quenching constant produced by Q. The k_{Ar} term actually consists of three individual terms representing diffusion to the wall and quenching by two-body and three-body collisions with Ar atoms.[30] The first-order decay rates of the metastable atom concentrations with H_2 and D_2 were measured relative to the decay rate of the $Ar(4s^3P_2)$ atoms with N_2. The ratio of the slopes of the logarithmic plots of the decay of metastable atom concentration vs added N_2 and H_2 (or D_2) gives the ratio of the rate constants, since the reaction times are the same. The data for quenching of $Ar(4s^3P_2)$ and $Ar(4s^3P_0)$ atoms by N_2, H_2, and D_2 are shown in Figure 2. The ratios of the slopes give $k_2(H_2)/k_2(N_2) = 1.67 \pm 0.08$, $k_2(D_2)/k_2(N_2) = 1.02 \pm 0.05$, $k_0(H_2)/k_2(N_2) = 2.68 \pm 0.15$, and $k_0(D_2)/k_2(N_2) = 1.61 \pm 0.09$. To obtain the absolute values of the rate constants given in Table 1, we adopted $(3.60 \pm 0.3) \times 10^{-11}$ cm^3 s^{-1} as the value for the rate constant for reaction 4.[28]

$$\mathrm{Ar}(4s^3P_2) + N_2 \rightarrow \mathrm{Ar} + N_2(C^3\Pi_u,\ v'=0-2=1000{:}207{:}35) \qquad (4)$$

The results are $k_2(H_2) = (6.0 \pm 0.8) \times 10^{-11}$ cm^3 s^{-1}, $k_2(D_2) = (3.7 \pm 0.5) \times 10^{-11}$ cm^3 s^{-1}, $k_0(H_2) = (9.6 \pm 1.5) \times 10^{-11}$ cm^3 s^{-1}, and $k_0(D_2) = (5.8 \pm 0.9) \times 10^{-11}$ cm^3 s^{-1}. Uncertainties for the k_Q values include the 8% uncertainty for the $k_2(N_2)$ and the 6% (8%) in the metastable densities.

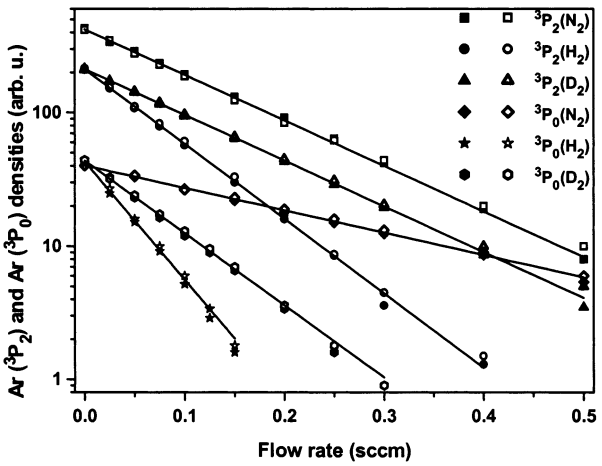

Figure 2. First-order decay plots of the $Ar(4s^3P_2)$ and $Ar(4s'^3P_0)$ concentrations in H_2 and D_2 with comparison to the decay in N_2 at 300 K in Grenoble flow tube. Solid and open characters are for increasing and decreasing flow rates, respectively. Solid lines are the best fits to exponential decay of the data points.

TABLE 1: Quenching Rate Constants of Ar ($4s^3P_2$) and Ar ($4s'^3P_0$) Atoms[a]

reagent (T)	Ar ($4s^3P_2$)	Ar ($4s'^3P_0$)	ref
H_2 (300)	$(6.0 \pm 0.8) \times 10^{-11}$	$(9.6 \pm 1.5) \times 10^{-11}$	this work: Grenoble
H_2 (300)		$(6.4 \pm 1.6) \times 10^{-11}$	this work: Orsay
H_2 (80)	$(0.76 \pm 0.23) \times 10^{-12}$	$(3.1 \pm 0.9) \times 10^{-12}$	this work: Orsay
D_2 (300)	$(3.7 \pm 0.5) \times 10^{-11}$	$(5.8 \pm 0.9) \times 10^{-11}$	this work: Grenoble
D_2 (80)	$\sim 0.53 \times 10^{-12}$	$\sim 2.2 \times 10^{-12}$	*b*
H_2 (300)	$(6.6 \pm 1.0) \times 10^{-11}$	$(7.8 \pm 1.2) \times 10^{-11}$	ref 1
D_2 (300)	$(4.7 \pm 0.7) \times 10^{-11}$	$(7.8 \pm 1.2) \times 10^{-11}$	ref 1
H_2 (300)	$(10.0 \pm 2.0) \times 10^{-11}$		ref 9
D_2 (300)	$(8.3 \pm 1.6) \times 10^{-11}$		ref 10
H_2 (0.043 eV)	6.2 ± 0.7 Å^2		ref 4[c]
D_2 (0.060 eV)	6.2 ± 0.7 Å^2		ref 4[c]

[a] All of the rate constants obtained in this work were measured relative to the $Ar(4s^3P_2) + N_2$ reaction rate constant $(3.6 \pm 0.3) \times 10^{-11}$cm^{3}s^{-1}. The ratio of $4s^3P_2$ and $4s'^3P_0$ rate constants for N_2 was also measured as 0.49 ± 0.03. [b] Deduced from $k(80)$ of H_2 assuming negligible isotopic effect on the cross sections of reactions 1 and 2. These estimates probably are upper limit values. [c] In this work cross sections are given.

The thermal quenching cross sections, $\sigma = k_Q/\langle v \rangle$, for reactions 1 and 2 are in the range of 3−5 Å^2 and quenching occurs in approximately one out of 10 collisions. For both metastable atoms, the quenching rate constants by H_2 are larger than for D_2 by a factor of 1.6. If the thermal cross sections are compared, the ratio of cross sections for H_2 vs D_2 is only 1.2, and the kinetic isotope effects on the cross sections for reactions 1 and 2 are small. The ratio of rate constants (or cross sections) for reactions 1 and 2 is 1.6 in favor of the $4s'^3P_0$ reactions for both H_2 and D_2 at 300 K.

We also measured the ratio of rate constants for N_2 reacting with $Ar(4s^3P_2)$ vs $Ar(4s'^3P_0)$ as $k_0(N_2)/k_2(N_2) = 0.49 \pm 0.03$, which gives $k_0(N_2) = (1.76 \pm 0.18) \times 10^{-11}$ cm^3 s^{-1}, in good agreement with other measurements.[1,28] The vibrational distribution in N_2 ($C^3\Pi_u$) state for the 300 K reaction is given in eq 5.[28]

$$\mathrm{Ar}(4s'^3P_0) + N_2 \rightarrow \mathrm{Ar} + N_2(C^3\Pi_u,\ v'=0-3=1000{:}369{:}276{:}208) \qquad (5)$$

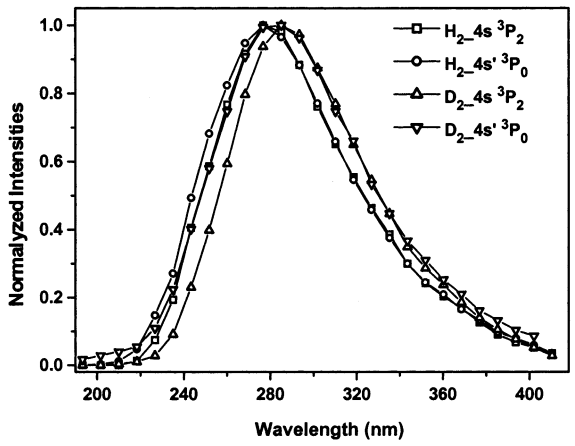

Figure 3. The ArH($B^2\Pi-X^2\Sigma^+$) and ArD($B^2\Pi-X^2\Sigma^+$) emission spectra from Ar($4s^3P_2$) and Ar($4s'^3P_0$) reactions, corrected for the spectral response of the detection system and normalized to their maxima. Note the slightly blue-shifted spectra from the Ar($4s'^3P_0$) reactions.

B. ArH Chemiluminescence Spectra and Reaction Rates at 300 K. Room-temperature experiments were done in the stationary-afterglow reactor to obtain the metastable state-selected chemiluminescence spectra from reactions 1 and 2. Optical pumping with the 772.4 nm line completely removed the $4s'^3P_0$ atom concentration and the ArH(B−X) and ArD(B−X) spectra from just $4s^3P_2$ atoms reacting with H_2 and D_2 could be obtained easily. These bound-free spectra, which are shown in Figure 3, are very similar; however, the ArD(B−X) spectrum is shifted slightly toward longer wavelengths.

The Ar($4s^3P_2$) atoms density was reduced to about 1% of its original level with 40% conversion to the $4s'^3P_0$ concentration. Thus, the spectra for reaction 2 were obtained with a 50:1 ratio of $4s'^3P_0$ to $4s^3P_2$ atoms. After the ratio of rate constants for the generation of the chemiluminescence was obtained, see below, the minor $4s^3P_2$ contribution to the spectrum was subtracted to obtain the pure ArH(B−X) and ArD(B−X) spectra shown in Figure 3 from the reaction of $4s'^3P_0$ atoms with H_2 and D_2. The slight blue extension of the ArH* and ArD* spectra from the Ar($4s'^3P_0$) reactions, relative to the spectra from the Ar($4s^3P_2$) reactions, is a consequence of the greater available energy for reaction 2.

Even though reactions 1 and 2 give nearly the same fluorescence spectra, it is possible to obtain the ratios of rate constants for emission from observing the total intensity, $I = k'_2[4s^3P_2][H_2] + k'_0[4s'^3P_0][H_2]$, for different relative concentrations of $4s^3P_2$ and $4s'^3P_0$ atoms; the primes denote the rate constants for chemiluminescence, whereas the unprimed rate constants are for total quenching. The relative concentrations were changed by optical pumping of $4s^3P_2$ atoms with 696.5 nm line and the rate constant ratio is given by eq 6.

$$\frac{k'_0}{k'_2} \equiv \frac{I^{wo}[^3P_2]^w - I^w[^3P_2]^{wo}}{I^w[^3P_0]^{wo} - I^{wo}[^3P_0]^w} \qquad (6)$$

The superscripts refer to the quantities with (w) and without (wo) laser optical pumping. The intensity was observed at the maximum of the spectrum, ∼280 nm, with and without pumping, and the metastable atom concentrations, $[^3P_2]$ and $[^3P_0]$, were measured by absorption during the observation gate. The average ratio from several experiments were $k'_0/k'_2 = 3.1 \pm 0.3$ for H_2 and $k'_0/k'_2 = 4.6 \pm 0.5$ for D_2. The higher energy metastable atom gives the strongest chemiluminescence from both H_2 and D_2.

To convert the k'_0/k'_2 ratios to absolute values of k'_0 and k'_2, the ArH(B) and ArD(B) emissions were compared to the $N_2(C^3\Pi_u-B^3\Pi_g)$ emission from reaction 4, with correction for the spectral response of the monochromator. These experiments were done in the Grenoble flow reactor at 300 K with a H_2/N_2 mixture consisting of 92.3% H_2 (or D_2) and 7.7% N_2. The chemiluminescence was observed 3 cm downstream of the reagent injection inlet. The integrated ArH(B−X) or ArD(B−X) emission intensities were compared to the 0−0 band of the $N_2(C)$ emission for a Ar($4s^3P_2$)/Ar($4s'^3P_0$) ratio of 7.5. The ratio of emission intensities is given by eq 7.

$$\frac{I_{ArH}}{I_{N_2(0,0)}} \equiv \left(\frac{1}{0.51}\right)\left(\frac{[H_2]}{[N_2]}\right)\left(\frac{k'_2[4s^3P_2] + k'_0[4s'^3P_0]}{k_2^{N_2}[4s^3P_2] + k_0^{N_2}[4s'^3P_0]}\right) \qquad (7)$$

The factor of $(0.51)^{-1}$ scales the $N_2(C;0-0)$ emission band to the total emission intensity from $N_2(C, v'=0)$; $k_2^{N_2}$ and $k_0^{N_2}$ are the rate constants for formation of $N_2(C, v'=0)$ from reactions 4 and 5, which have values of 2.90×10^{-11} and 0.75×10^{-11} cm^3 s^{-1}, respectively.[28,31] Since the k_0'/k_2' values for H_2 and D_2 are known, the experimental intensity ratios from H_2 and D_2 reactions can be converted to k_2' values after the $4s^3P_2$ and $4s'^3P_0$ concentrations are measured. The measured rate constants for ArH(B) and ArD(B) formation are summarized in Table 2, with uncertainties that are derived from 10% for $k_2^{N_2}$ and 12% (15%) for k_2' (k_0'), respectively. The branching fractions at 300 K for chemiluminescence, k'_2/k_2 and k'_0/k_0, are 0.075 and 0.15 for H_2 and 0.11 and 0.33 for D_2 for reactions 1 and 2, respectively. These branching fractions increase significantly for the higher energy metastable atoms and for D_2 relative to H_2.

C. Total Quenching Rate Measurements at 80 K. All experiments at 80 K were done in the flow reactor at Orsay. To ensure equivalence with the Grenoble reactor, the rate constant for reaction 1 at 300 K was measured relative to reaction 4, using the fixed-point observation method. The rate constant, $k_0(H_2)$ was $(6.4 \pm 1.6) \times 10^{-11}$ cm^3 s^{-1}, which is in good agreement with the Grenoble result. We also measured $k_2'(H_2)$ and $k_0'(H_2)$ at 300 K by comparison of the ArH(B−X) and $N_2(C, v'=0 \rightarrow B)$ emission intensities as described in section III.B and found $k_2'(H_2) = (0.52 \pm 0.12) \times 10^{-11}$ cm^3 s^{-1} and $k_0'(H_2) = (1.62 \pm 0.40) \times 10^{-11}$ cm^3 s^{-1}, which also agree with the Grenoble results.

Cooling the flow reactor, at fixed pressure, from 300 to 80 K, increases the gas density as T^{-1} and decreases the mean flow velocity as T. These modifications of flow parameters greatly change the interaction time between the discharge zone and the observation point, and the two- and three-body collisional quenching frequencies of the Ar($4s^3P_2$) and Ar($4s'^3P_0$) atoms, even in the absence of added reagent. Figure 4 shows the density ratio $[Ar(^3P_2)]/[Ar(^3P_0)]$ at the observation window versus the argon flow rate, ρ, at both 300 and 80 K. The pumping speed (l/s) increased slightly with the pressure and when ρ rose from 1.3 to 5.6 slm, the total pressure varied from 0.35 to 0.95 Torr at 300 K and from 0.32 to 0.83 at 80 K. Simultaneously, the mean flow velocity in the reaction tube increased from 26 to 42 m/s at 300 K and from 6.8 to 11 m/s at 80 K. The most obvious result is that with reduction of temperature the relative concentration of $4s^3P_2$ atoms at the second window, where the chemiluminescence intensity was measured, decreased by ∼20, relative to the $4s'^3P_0$ atom concentration, for ρ=3 slm (p= 0.60 Torr at 300 K and 0.51 Torr at 80 K). In fact, the concentration

TABLE 2: Rate Constants and Branching Fractions for ArH* and ArD* Formation

	Ar ($4s^3P_2$)		Ar($4s'^3P_0$)	
reagent (T)	k'_2	k'_2/k_2	k'_0	k'_0/k_0
H_2 (300)−Grenoble	$(0.45 \pm 0.10) \times 10^{-11}$	0.075	$(1.41 \pm 0.35) \times 10^{-11}$	0.15
H_2 (300)−Orsay	$(0.52 \pm 0.12) \times 10^{-11}$ (a)	0.087 (b)	$(1.62 \pm 0.40) \times 10^{-11}$	0.16 (b)
H_2 (80)−Orsay	$\sim 3 \times 10^{-14}$ (c)	0.04	$(1.0 \pm 0.35) \times 10^{-12}$	0.32
D_2 (300)−Grenoble	$(0.40 \pm 0.08) \times 10^{-11}$	0.11	$(1.90 + 0.47) \times 10^{-11}$	0.33
D_2 (80)−Orsay	$\sim 1 \times 10^{-15}$ (c)	0.002 (d)	$(0.15 \pm 0.05) \times 10^{-12}$ (e)	0.07 (d)

[a] The ratio $k_0'/k_2' = 3.1$ measured in Grenoble was used to obtain these k' values. [b] The total quenching constant measured in Grenoble was used to obtain this branching fraction. [c] Deduced from $k'_0(80)$ and the ratio $k'_0(80)/k'_2(80)$ cited in the text. [d] Large uncertainties (~100%) are associated to these ratios, because $k_2(80)$ and $k_0(80)$ were estimated (see text). [e] This absolute value was obtained from the 300 K measurement of k'_0 at Grenoble, and the ratio cited in the text for $k'_0(80\text{ K})/k'_0(300\text{ K})$.

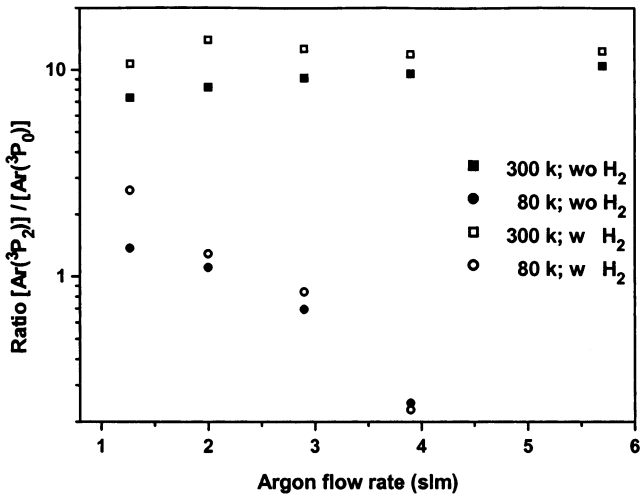

Figure 4. Variation of the ratio $[Ar(4s^3P_2)]/[Ar(4s'^3P_0)]$ versus argon flow rate at 300 and 80 K, without and with 0.45 sccm of H_2 added.

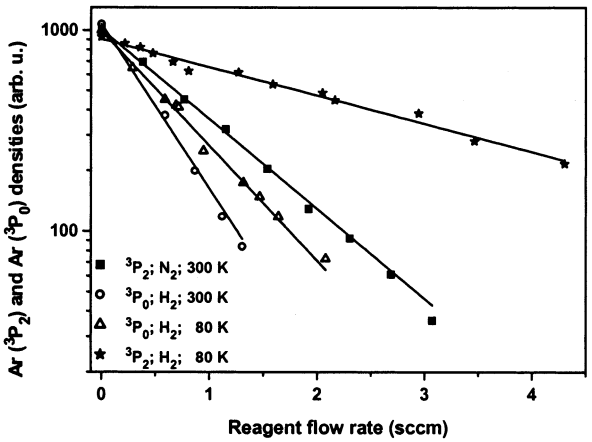

Figure 5. First-order decay plots of $Ar(4s^3P_2)$ and $Ar(4s'^3P_0)$ concentrations in H_2 with comparison to the decay of $Ar(4s^3P_2)$ in N_2 at 300 K in the Orsay flow tube. Solid lines are the best fits to exponential decay of data points.

of $4s'^3P_0$ atoms was dominant at 80 K. This dramatic change in the relative densities at 80 K is due to the reduction of the $4s^3P_2$ density, because the $4s'^3P_0$ density remained nearly constant at low flow rate ($\rho = 1.27$ slm; $p = 0.32$ Torr) and was reduced by 50% at high flow rate ($\rho = 3.9$ slm; p ≅ 0.7 Torr), relative to 300 K conditions. Golde[32] also observed a similar trend for the relative concentrations, as well as an overall increase in the concentration of both metastable atoms in studies at 220 K. Since the relative metastable atom concentration in the cooled stationary reactor[31] was about the same as that at 300 K, the relative increase in the $Ar(4s'^3P_0)$ concentration must be associated with differences in decay rates and not with change in generation mechanism. In the Orsay reactor, the transit time between the discharge zone and the observation point was about 10 ms at 300 K and 40 ms at 80 K, and we must consider the changes with T of Ar density, the rate of diffusion, and the two- and three-body quenching rates. At fixed pressure, the diffusion constant should vary as $T^{1.5}$, two-body quenching frequency as $\sigma_2(T) \times T^{-0.5}$, and three-body quenching frequency as $\sigma_3(T) \times T^{-1}$. Taking into account the 4 times longer transit time of metastable atoms, the loss term by diffusion should be reduced by a factor of 2, whereas, for $\sigma_2(T)$ and $\sigma_3(T)$ independent of T, the loss terms by two- and three-body collisions should increase by 8 and 16, respectively. We should emphasis that according to eq 3, the metastable atoms densities depend exponentially on these terms. Usually, two-body quenching cross sections σ_2 are not a strong function of temperature, thus our results seems to indicate that, at 80 K, the three-body quenching becomes very small for $4s'^3P_0$ atoms, whereas the rate is still significant for $4s^3P_2$ atoms.

The total quenching rate constants for reactions 1 and 2 with H_2 were measured at 80 K by comparison with quenching by N_2 at 300 K, reaction 4, and the first-order quenching plots are deduced from the slope of metastable atom density versus the reactant flow rate, as shown in Figure 5. The metastable atom concentrations were measured by atomic absorption, just as for the room-temperature experiments. Given that in eq 3 [Q], the density of reagent, is $[Q] \propto \rho_Q/w$, where ρ_Q is the reagent flow rate and w is the mean flow velocity in the reaction chamber, and the interaction time is $t \propto 1/w$; therefore, the slope of each curve must be multiplied by w^2 to scale with k_Q. In Figure 5, w was 30 m/s at 300 K and 8.5 and 7.9 m/s at 80 K for $^3P_0$ and $^3P_2$ measurements, respectively. We then deduce $k_2(H_2) = (0.76 \pm 0.25) \times 10^{-12}$ cm^3 s^{-1} and $k_0(H_2) = (3.1 \pm 0.9) \times 10^{-12}$ cm^3 s^{-1} at 80 K. The 30% uncertainty considered for these values is due to the 10% uncertainty in $k_2(N_2)$ value at 300 K and the 20% statistical experimental uncertainties (12% for the slopes ratio and 8% on determination of each flow velocity) reactions (1 and 2 are both much slower at 80 K, but the effect is a factor of 80 for the $4s^3P_2$ atoms and only a factor of 30 for the $4s'^3P_0$ atoms.

D. ArH Chemiluminescence Spectra and Reaction Rates at 80 K. Chemiluminescence spectra obtained at 300 and 80 K in the Orsay reactor, with 5 nm monochromator steps, are shown in Figure 6. The slight difference observed between the 300 K spectrum of Figure 6 with the one obtained in Grenoble (Figure 3) comes from the different spectral response calibration procedure of the monochromators used in these two laboratories. Both spectra of Figure 6 are quite similar and no significant temperature dependence can be detected. It should be remembered that the 300 K spectrum is dominated by reaction 1, whereas the 80 K spectrum is from reaction 2. Just as for the 300 K experiments, we first determined the ratio k_0'/k_2' at 80 K. Since optical pumping was not possible at Orsay, we used

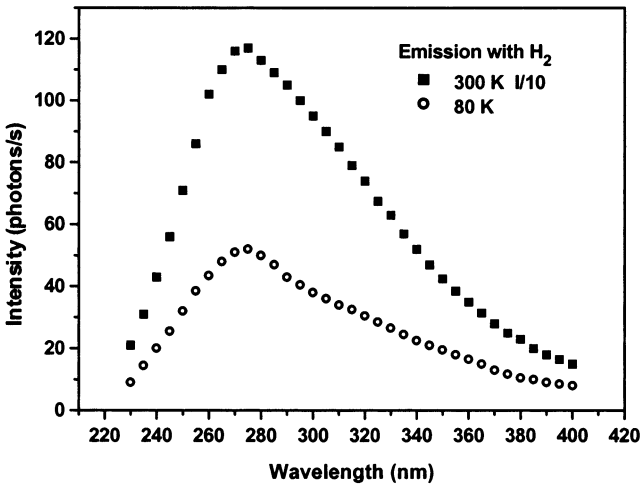

Figure 6. Chemiluminescence spectra from Orsay reactor at 300 and 80 K, corrected for the spectral response of the detection system.

the dependence of the $4s^3P_2$ density on argon flow rate, shown in Figure 4, to change the ratio of metastable concentrations. At fixed hydrogen flow rate ρ_{H_2}, the intensity of the chemiluminescence is given by

$$I_{ArH} \propto [H_2]^*(k'_2[4s^3P_2] + k'_0[4s'^3P_0]) \propto \frac{\rho_{H_2}}{w}{}^*k'_0[^3P_0]^*\left(1 + \frac{k'_2}{k'_0}{}^*\frac{[^3P_2]}{[^3P_0]}\right) \quad (8)$$

where w is the gas flow velocity, deduced from measured values of the argon flow rate and the gas pressure. At fixed H_2 flow rate of 0.45 sccm (standard cubic cm per minute), values of I_{ArH}, $[4s^3P_2]$, $[4s^3P_0]$, and total pressure were measured for different argon flow rates ranging between 1.2 and 4 slm. Then for different flow rates, $I_{ArH}w/[^3P_0]$ was plotted vs $[^3P_2]/[^3P_0]$. The slope of this linear plot gave $k_0'/k_2' = 30 \pm 8$ and 120 ± 30 for H_2 and D_2, respectively.

The slow reaction rate for reaction 1 at 80 K and its smaller branching fraction for chemiluminescence, compared to reaction 2, plus comparable densities of both metastable states, made observation of the ArH(B−X) emission from Ar $(4s^3P_2)$ impossible, and we only measured $k'_0(H_2)$ and $k'_0(D_2)$ at 80 K. Experiments were done by comparing the ArH* (or ArD*) intensities at 300 K to those at 80 K for the same flow rate of H_2. Using eq 8 at both 300 and 80 K and neglecting the contribution from $Ar[4s^3P_2]$ atoms at 80 K, the ratio of the ArH* intensities, combined with the experimental values of flow velocities and metastables densities, provided the ratio of the rate constants $(k'_0{}^{300}/k'_0{}^{80})_{H2} = 16 \pm 3$ and $(k'_0{}^{300}/k'_0{}^{80})_{D2} = 125 \pm 25$. These ratios lead to rate constants $k'_0{}^{80}$ of $(1.0 \pm 0.35) \times 10^{-12}$ and $(0.15 \pm 0.05) \times 10^{-12}$ cm^3 s^{-1} for H_2 and D_2, respectively. The ratios quoted above for k_0'/k_2' at 80 K can be used to obtain the k_2' values given in Table 2 for H_2 and D_2. The branching fraction for ArH* formation at 80 K are 0.32 from reaction 2 and 0.04 for reaction 1. Although the latter number may have a large uncertainty, the branching fraction for the $Ar(4s^3P_2)$ reaction declines by a factor of 2,whereas that for $Ar(4s'^3P_0)$ increases by a factor of 2, relative to the 300 K values. The branching fractions for ArD* formation at 80 K can only be estimated, because $k_0(D_2)$ and $k_2(D_2)$ were not measured. If we assume that the isotope effect on the quenching cross sections are negligible (as for the 300 K quenching) then $k_2(D_2) = 0.53 \times 10^{-12}$ and $k_0(D_2) = 2.2 \times 10^{-12}$ cm^3 s^{-1} are deduced and the branching fractions would be 0.002 and 0.06 for $4s^3P_2$ and $4s'^3P_0$, respectively. These estimates probably are lower limits because isotope effects may exist at low temperature for the cross sections. Nevertheless, it seems that the branching fractions for ArD* decreases at 80 K for both reactions 1 and 2.

IV. Discussion

A. Assignment of the Chemiluminescence to ArH(B) and ArD(B). The justification for assigning the chemiluminescence from reactions 1 and 2 to the ArH(B−X) emission is summarized below.

1. Muschlitz and co-workers[5] showed that the chemiluminescence spectrum did not match the $H_2(a\ ^3\Sigma^+_g \rightarrow b\ ^3\Sigma^+_u)$ continuum emission.

2. Chemiluminescence spectra obtained in this work from reactions 1 and 2 are very similar to those resulting from charge exchange reaction between ArH^+ and Cs,[18] and from the $H_2(B\ ^1\Sigma^+_u, v' \geq 3)$ + Ar reaction.[11]

3. The chemiluminescence branching fraction for $4s'^3P_0$ + H_2 actually increased with reduction of temperature. Formation of $H_2(a\ ^3\Sigma^+_g)$ requires 95076 cm^{-1} and the energy of $Ar(4s'^3P_0)$ is 94553 cm^{-1}. It seems unlikely that formation of $H_2(a^3\Sigma^+_g)$ would increase relative to the other dark channels at reduced temperature.

4. The excitation of $H_2(a^3\Sigma^+_g)$ and $D_2(a^3\Sigma^+_g)$ requires 95076 and 95348 cm^{-1} of energy, yet the branching fractions for chemiluminescence are larger for D_2 than those for H_2 for both metastable atom reactions at 300 K.

All of these arguments support a reactive quenching mechanism giving ArH* as the source for the chemiluminescence. Although bound-free spectra have intrinsically low information content, some features can be deduced by comparison to the experimental spectra from the ArH^+ + Cs reaction and the spectral simulations given in ref 18.

The ArH(B) and ArD(B) molecules formed by reaction 1 should be in $v' = 0$ due to the energy constraint. Since the lower state potential is the same for both ArH(X) and ArD(X), the ArD* spectrum should be red shifted because of the zero point energy difference of ArH(B) and ArD(B), which is 290 cm^{-1}. Inspection of the spectra in Figure 3 confirms this expectation. Reaction 2 is endoergic by only 0.1 eV for formation of ArD(B; $v'=1$) and a small population in $v'=1$ could be expected. According to the simulation given in ref 18, the emission from $v'=1$ will add emission intensity mainly to the short wavelengths side of the $v'=0$ spectrum. This is exactly what we observed in the spectra from reaction 2; see Figure 3.

At 300 K, the branching fraction for chemiluminescence seems to be systematically larger from the D_2 reactions than from H_2 reactions. Before attributing this to isotopic effects on the reaction dynamics, the possibility of emission from the $ArD(C\ ^2\Sigma^+)$ state at 300 K needs to be examined. The B and C states are nearly degenerate and contributions from the C state would not be detected from the appearance of a characteristic modification in the spectra. The calculated predissociation rate is sensitive to isotope effects and the ArD(C) state is predicted to have a predissociation lifetime of 0.6 ns versus a radiative lifetime of 7 ns.[13] Thus, a 10% contribution to the ArD* spectrum is possible if the ArD* molecules are formed equally in the B and C states. In contrast, the $ArH(C\ ^2\Sigma^+)$ state is more than 99% predissociated.[13,15] The larger branching fractions at 300 K for ArD* probably are not a consequence of $ArD(C\ ^2\Sigma^+)$ formation. Actually, the rate constants for formation of ArD* and ArH* are similar at 300 K, and the larger branching fractions for ArD* are mainly because the quenching constants are smaller

for D_2 than H_2. At 80 K, the difference between D_2 and H_2 reactions seems larger, but inverted. Although the uncertainties are large, the branching factions and k_2' and k_0' values seem smaller for D_2 than H_2 at 80 K. The effect is more pronounced for $Ar(4s^3P_2)$ than for $Ar(4s'^3P_0)$, which could be a consequence of the 0.03 eV higher endoexergicity for ArD* formation. In their molecular beam study with an assumed metastable atom composition of 5:1 for $Ar(4s^3P_2)/Ar(4s'^3P_0)$, Lishawa et al.[5] reported a strong energy dependent decrease for the cross sections of ArH* and ArD* formation over the 0.07−0.16 eV range. They suggested a threshold energy of 0.065 ± 0.009 eV for the chemiluminescence of both H_2 and D_2 reactions. The greater reduction of k_2' (80) than $k_0'(80)$ is consistent with the beam data. However, even for the exoergic $Ar(4s'^3P_0)$ reactions, the rate constants for ArH* and ArD* formation decreases by factors of 16 (H_2) and 125 (D_2), when T is reduced from 300 to 80 K, and small barriers must also exist for reaction 2.

B. The Overall Reaction Mechanism. If the chemiluminescence for reactions 1 and 2 is accepted to arise from ArH(B) and ArD(B,C), then it seems logical to assign the nonluminescence part of the reaction mainly to $ArH(A^2\Sigma^+)$ formation, which subsequently predissociates, rather than to a formal energy transfer event to the $H_2(b^3\Sigma^+_u)$ dissociative state. Allison et al. [4] report that the quenching cross section of metastable Ar atoms by D_2 increased over the 0.48−0.73 eV range, and we find increases in the thermal cross sections by factors of 41 and 16 for H_2 with Ar(4s) and Ar(4s′) atoms, respectively, from 80 to 300 K. These results imply that small energy barriers exist in the entrance channels for total quenching, as well as for ArH* and ArD* formation. Although the energy transfer to the dissociative $H_2(b\ ^3\Sigma^+_u)$ state could have an energy constraint, the results seem more consistent with a chemical interaction mechanism for quenching. The calculations of Blickensderfer et al.[33] suggest that the triplet state Ar(4s) atoms will have attractive interactions with H_2, and they suggest an exit channel from C_{2v} geometry that correlates directly to dissociative products. Thus, formation of ArH(A) followed by predissociation may not occur in all collision events. On the other hand, excited-state alkali metal atoms do react with H_2 by a collinear abstraction mechanism.[23,24] One also should not forget that Ar^+, Kr^+ and Xe^+ ions react with H_2 to give ArH^+, KrH^+, and XeH^+.[34]

V. Conclusion

The current assignment of the UV chemiluminescence from the reactions of $Ar(4s,^3P_2)$ and $Ar(4s',^3P_0)$ atoms with H_2 to the formation of $ArH(B^2\Pi)$ removes one of the remaining puzzles associated with the quenching reactions of metastable Ar atoms by small molecules. Chemical reactions, as well as energy transfer processes, are frequently important for quenching of electronically excited atoms. The branching fraction at 300 K for $ArH(B^2\Pi)$ formation is two times larger for $Ar(4s',^3P_0)$ than for $Ar(4s,^3P_2)$ atoms. The branching fraction for ArD* formation is higher than for ArH* formation at 300 K, but it is lower at 80 K. The quenching rate constants for H_2 decline by factors of 80 and 30 at 80 K for $Ar(4s^3P_2)$ and $Ar(4s'^3P_0)$ atoms, respectively; however, $ArH(B^2\Pi)$ is still a significant product at 80 K.

The $Ar(4s'^3P_0)$ atoms decay much more slowly than the $Ar(4s^3P_2)$ atoms in pure Ar at 80 K. This unexpected result, based on decay rates at 300 K, seems to be a consequence of a much smaller three-body rate constant for the $Ar(4s'^3P_0)$ atoms relative to the $Ar(4s^3P_2)$ atoms at 80 K. Systematic studies of the decay rates of both metastables as a function of temperature are needed to verify this suggestion and to understand the origin of the difference in three-body rates.

References and Notes

(1) Velazco, J. E.; Kolts, J. H.; Setser, D. W. *J. Chem. Phys.* **1978**, *69*, 4357.
(2) Chen, X.; Setser, D. W. *J. Phys. Chem.* **1991**, *95*, 8473.
(3) Balamuta, J.; Golde, M. F. *J. Chem. Phys.* **1982**, 76, 2430.
(4) Allison, W.; Sheldon, J. W.; Muschlitz, E. E., Jr. *J. Phys. B: At. Mol. Phys.* **1981**, *14*, 4587.
(5) Lishawa, C. R.; Feldstein, J. W.; Stewart, T. N.; Muschlitz, E. E., Jr. *J. Chem. Phys.* **1985**, *83*, 133.
(6) Nguyen, T. D.; Sadeghi, N. *Phys. Rev. A* **1978**, *18*, 1388.
(7) Derourd, J.; Nguyen, T. D.; Sadeghi, N. *J. Chem. Phys.* **1980**, *72*, 6698.
(8) Dreiling, T. D.; Sadeghi, N. *J. Phys. (Paris)* **1983**, *44*, 1007.
(9) Bourne, M.; Dutuit, O.; LeCalvé, J. *J. Chem. Phys.* **1975**, *63*, 1668.
(10) Bourne, M.; LeCalvé, J. *J. Chem. Phys.* **1973**, *58*, 1452.
(11) Möller, T.; Beland M.; Zimmerer, G. *Chem. Phys. Lett.* **1987**, *13A*, 351.
(12) Theodorakopoulous, G.; Petsalakis, I. D.; Buenker, R. *J. Mol. Phys.* **1990**, *71*, 1055.
(13) Theodorakopoulous, G.; Petsalakis, I. D. *J. Chem. Phys.* **1994**, *101*, 194.
(14) Petsalakis, I. D.; Theodorakopoulous, G. *J. Phys. B: At. Mol. Phys.* **1994**, *27*, 4483; *J. Phys. B: At. Mol. Phys.* **1992**, *25*, 5353.
(15) van Hemert, M. C.; Dohmann, H.; Peyerimhoff, S. D. *Chem. Phys.* **1986**, *110*, 55.
(16) Dabrowski, I.; Tokoryk, D. W.; Lipson, R. H.; Watson, J. K. G. *J. Mol. Spectrosc.* **1998**, *189*, 110.
(17) Bruckmeier, R.; Wunderlich, C.; Figger, H. *Phys. Rev. A* **1995**, *52*, 334.
(18) Wunderlich, C.; Witzel, B.; Brockmeier, R.; Figger, H. *Can. J. Phys.* **1994**, *72*, 1236.
(19) Wunderlich, C.; Betz, V.; Bruckmeier, R.; Figger, H. *J. Chem. Phys.* **1993**, *98*, 9362.
(20) Fink, E. H.; Wallach, D.; Moore, C. B. *J. Chem. Phys.* **1972**, *56*, 3608.
(21) McNeely, J. R.; Hurst, G. S.; Wagner, E. B.; Payne, M. G. *J. Chem. Phys.* **1975**, *63*, 2717.
(22) Alekseev, V. A.; Setser, D. W. *J. Phys. Chem. A.* **1999**, *103*, 8396.
(23) (a) Liu, D. K.; Lin, K. C. *J. Chem. Phys.* **1990**, *105*, 9121. (b) Wong, T. H.; Kleiber, D. D.; Yang, K. H. *J. Chem. Phys.* **1999**, *110*, 6743.
(24) (a) L'Hermite, J. M.; Rahmat, G.; Vetter, R. *J. Chem. Phys.* **1990**, *93*, 434. (b) L'Hermite, J. M. *J. Chem. Phys.* **1992**, *97*, 6215. (c) Huang, X.; Zhao, J.; Xing, G.; Wong, X.; Bersohn, R. *J. Chem. Phys.* **1996**, *104*, 1338.
(25) Lavrov, B. P.; Melnikov, A. S.; Käning M.; Röpcke, *J. Phys. Rev. E* **1999**, *59*, 3526.
(26) Lorenzen, J.; Hotop, H.; Ruf, M. W.; Morgner, H. *Z. Phys. A* **1980**, *297*, 19.
(27) deSousa, A. R.; Touzeau, M.; Petitdider, M. *Chem. Phys. Lett.* **1985**, *121*, 423.
(28) Sadeghi, N.; Cheaib M.; Setser, D. W. *J. Chem. Phys.* **1989**, *90*, 219.
(29) Ohebsian, D.; Sadeghi, N.; Trassy C.; Mermet, J. M. *Opt. Commun.* **1980**, *32*, 81.
(30) Kolts, J. H.; Setser, D. W. *J. Chem. Phys.* **1978**, *68*, 4848. Ellis, E.; Twiddy, N. D. *J. Phys. B: At. Mol. Phys.* **1969**, *2*, 1366.
(31) Nguyen, T. D.; Sadeghi, N. *Chem. Phys.* **1983**, *79*, 41.
(32) Golde, M. F.; Ho, Y. S. J. *Chem. Phys.* **1985**, *82*, 3160.
(33) Blickensderfer, R. P.; Sunll, K. K.; Jordan, K. D. *J. Phys. Chem.* **1983**, *87*, 1480.
(34) Ervin, K. M.; Armentrout, P. B. *J. Chem. Phys.* **1989**, *90*, 118; *J. Chem. Phys.* **1986**, *85*, 6380.